H1prelim-08-072 Submitted to

XVI International Workshop on Deep-Inelastic Scattering, DIS2008, April 7-11, 2008, London
Parallel Session **Heavy Flavours**

Electronic Access:https://www-h1.desy.de/publications/H1preliminary.short_list.html

D^* production at low Q^2 with the H1 detector

H1 Collaboration

Abstract

Inclusive production of D^* mesons in deep inelastic scattering at HERA is studied. The data were taken with the H1 detector in the years 2004 to 2007 and correspond to an integrated luminosity of 347 pb^{-1} increasing the available data by a factor 10 compared to the previous publication. This analysis covers the region $5 < Q^2 < 100$ GeV^2 in the photon virtuality and $0.02 < y < 0.7$ in the inelasticity. The visible range for the D^*meson is $p_T(D^\star) > 1.5$ GeV and $|\eta(D^\star)| < 1.5$. Single and double differential cross sections are compared to prediction from the NLO calculation HVQDIS and the LO MC programs RAPGAP and CASCADE.

1 D* in DIS at H1

The analysed periods span from beginning of the year 2004 until the end of the high energy running 2007. The total collected luminosity $\mathcal{L}$ during this period amounts to $\mathcal{L} = (347.7 \pm 11.1)$ pb^{-1}. The luminosity has been corrected for prescales and satellite bunch contributions. Only D^*-Mesons decaying in the golden channel $D^{\star\pm} \to D^0\pi^{\pm}_{\text{slow}} \to K^{\mp}\pi^{\pm}\pi^{\pm}_{\text{slow}}$ are taken into account in the analysis. The slow pion is created just above its mass threshold and therefore its transverse momentum p_t is small. In order to calculate the total D^*-meson production cross section the branching ratio by other experiments is needed. To determine the number of D^*-mesons the ΔM-distribution is plotted:

$$\Delta M = M(K\pi\pi_{\text{slow}}) - M(K\pi) \ . \tag{1}$$

Applying the complete event selection for deep inelastic scattering (DIS) and for D^*-meson candidates one gets the ΔM- and $M(D^0)$-distributions, which are shown in the figure 1. From these plots one expect a large number of D^*-mesons. Due to the limited acceptance of the H1

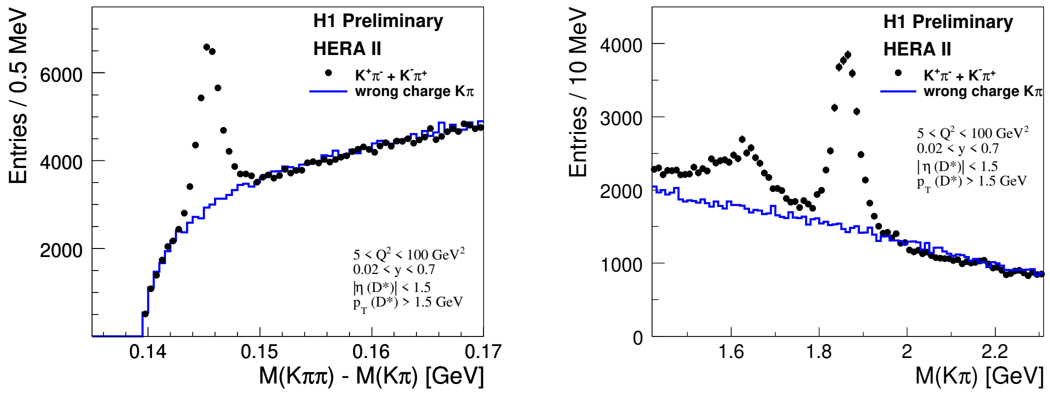

Figure 1: Distribution of the ΔM and D^0-Mass of all D^*-meson candidates, which are found in the presented analysis. The wrong charged background is also shown as the blue lined histogram.

detector the cross section is only measured in the visible kinematic region. The definition of the visibility is given in the table 1.

Name	Wert
$p_t(D^\star)$	> 1.5 GeV
$\lvert\eta(D^\star)\rvert$	< 1.5
Virtuality	$5 < Q^2 < 100$ GeV^2
Inelasticity	$0.02 < y < 0.70$

Table 1: Definition of the visible range.

The selection cuts of the analysis are listed in the following:

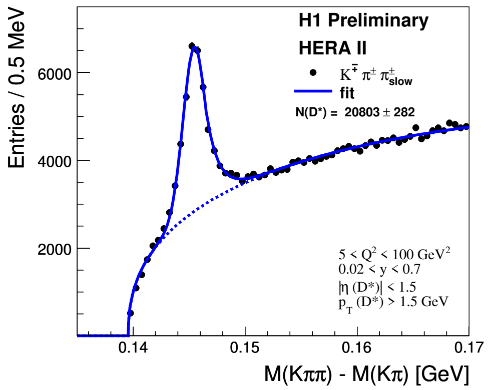

Figure 2: Distribution of the ΔM -Mass of all D^*-meson candidates, which are found in the presented analysis.

Name	Wert
$p_t(D^\star)$	$>$ 1.5 GeV
$\lvert\eta(D^\star)\rvert$	$<$ 1.5
$p_t(K)$	$>$ 0.3 GeV
$p_t(\pi)$	$>$ 0.3 GeV
$p_t(\pi_{\mathrm{slow}})$	$>$ 0.120 GeV
$p_t(K) + p_t(\pi)$	$>$ 2.0 GeV
$\lvert M(K\pi) - M(D^0)\rvert$	$<$ 0.08 GeV
ΔM	$<$ 0.170 GeV

Table 2: Selection cuts on the invariant masses and the transverse momenta of the tracks of decay particles.

1.1 Determination of the Cross-Section

For the calculation of the cross-section the following formula is used:

$$\sigma_{\mathrm{tot}}^{\mathrm{vis}} = \frac{N_{D^\star} \cdot (1 - r)}{\mathcal{L} \cdot \mathcal{B}(D^\star \to K\pi\pi_{\mathrm{slow}}) \cdot \epsilon \cdot (1 - \delta_{rad})} \ . \tag{2}$$

For a cross section determination the number of D^*-mesons $N_{D^\star}$ is corrected by $r = 4\%$ to take the reflections into acount. The presented cross sections are at Born-level therefor a radiative correction $(1 - \delta_{rad})$ is applied.

1.2 Total Cross-Section

The total visible cross section has been measured to be:

$$\sigma_{\mathrm{vis}}^{\mathrm{tot}}(e^\pm p \to e^\pm D^{\star\pm} X) = 4.85 \pm 0.07\ (\mathrm{stat.}) \pm 0.42\ (\mathrm{syst.})\ \mathrm{nb}. \tag{3}$$

The total systematic uncertainty error is $\approx\ 8.7\%$. The visible region is defined in table 1. For the same visible region RAPGAP (CTEQ6ll) yields a cross section of $\sigma_{\mathrm{vis}}^{\mathrm{tot}} = 4.89$ nb and

$\sigma_{\text{vis}}^{\text{tot}} = 3.65$ nb if used with the CTEQ65m parametrization for the proton PDF. CASCADE yields a cross section of $\sigma_{\text{vis}}^{\text{tot}} = 4.72$ nb. In both cases a charm mass of 1.5 GeV has been used. In addition the comparison to the NLO calculation made HVQDIS is shown in the cross section plots. HVQDIS is used with two different proton PDFs namely MRST2004FF3nlo and CTEQ5f3. In the case of the CTEQ5f3 HVQDIS yields a cross section of $\sigma_{\text{vis}}^{\text{tot}} = 4.43 \pm_{0.47}^{0.69}$ nb where as $\sigma_{\text{vis}}^{\text{tot}} = 4.17 \pm_{0.37}^{0.59}$ nb for the MRST PDF is calculated. The error is calculated from

name	interval
charm mass	$1.3 < m_c < 1.6$ GeV
scale $\mu_0^2 = Q^2 + 4m_c^2$	$1 < \mu_{r,f}/\mu_0 < 4$
fragmentation	$2.9 < \alpha(\text{Kartvelishvili}) < 3.7$

Table 3: Parameter variations used for the error estimation of HVQDIS.

variations of four parameters given in table 3.
In order to distinguish the different models the ratio R is calculated for the variable Y and shown for the single differential plots:

$$R = \frac{1/\sigma_{tot,vis}^{calc} \cdot \frac{d\sigma^{calc}}{dY}}{1/\sigma_{tot,vis}^{data} \cdot \frac{d\sigma^{data}}{dY}} \ . \qquad (4)$$

1.3 Differential Cross-Section

In the following plots the results of the measurement are given:

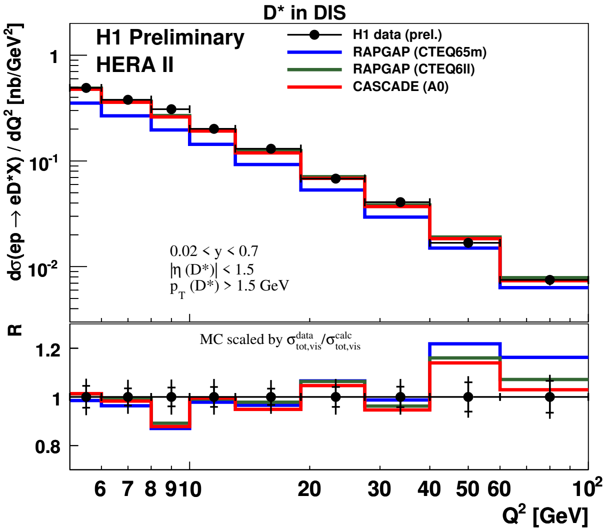

Figure 3: Differential cross section as a function of Q^2 compared with RAPGAP using two different Proton PDF's and CASCADE.

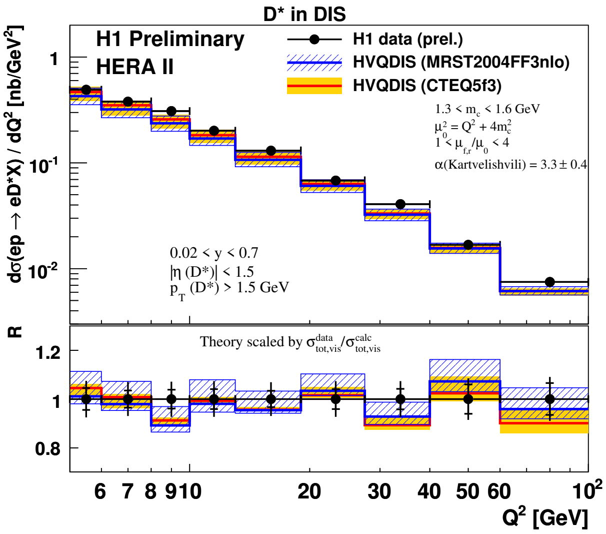

Figure 4: Differential cross section as a function of Q^2 compared with the NLO calculation (HVQDIS) with two different Proton PDF's.

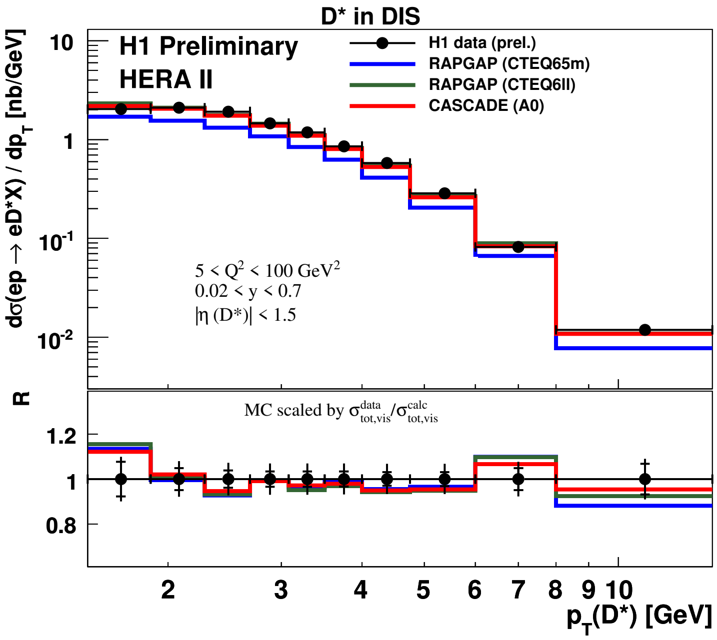

Figure 5: Differential cross section as a function of p_T of the D^*-mesons compared with RAPGAP using two different Proton PDF's and CASCADE.

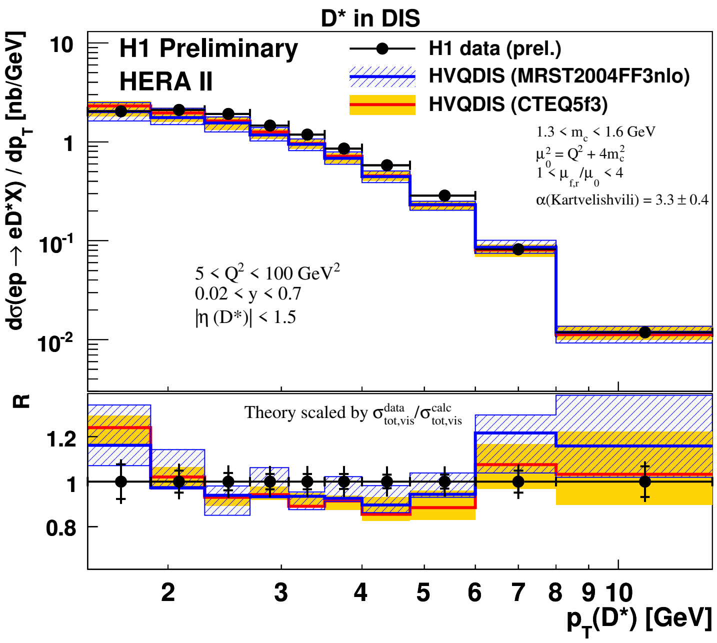

Figure 6: Differential cross section as a function of p_T of the D^*-mesons compared with the NLO calculation (HVQDIS) with two different Proton PDF's.

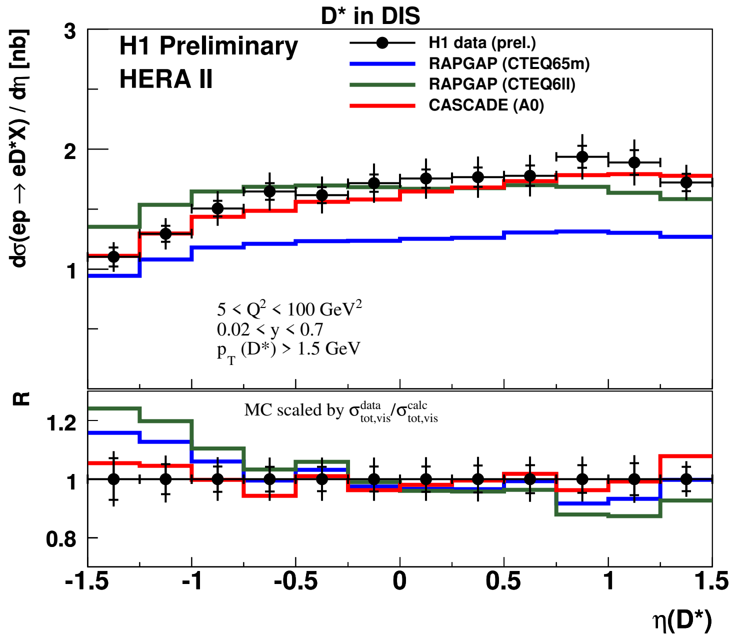

Figure 7: Differential cross sections as a function of the pseudorapidity η_{D^*} of the D^*-mesons compared with RAPGAP using two different Proton PDF's and CASCADE.

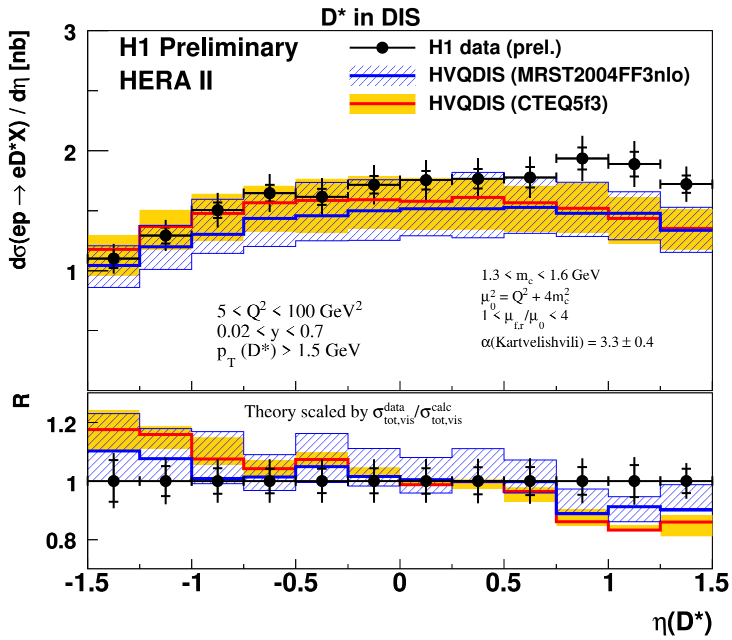

Figure 8: Differential cross sections as a function of the pseudorapidity η_{D^*} of the D^*-mesons compared with the NLO calculation (HVQDIS) with two different Proton PDF's.

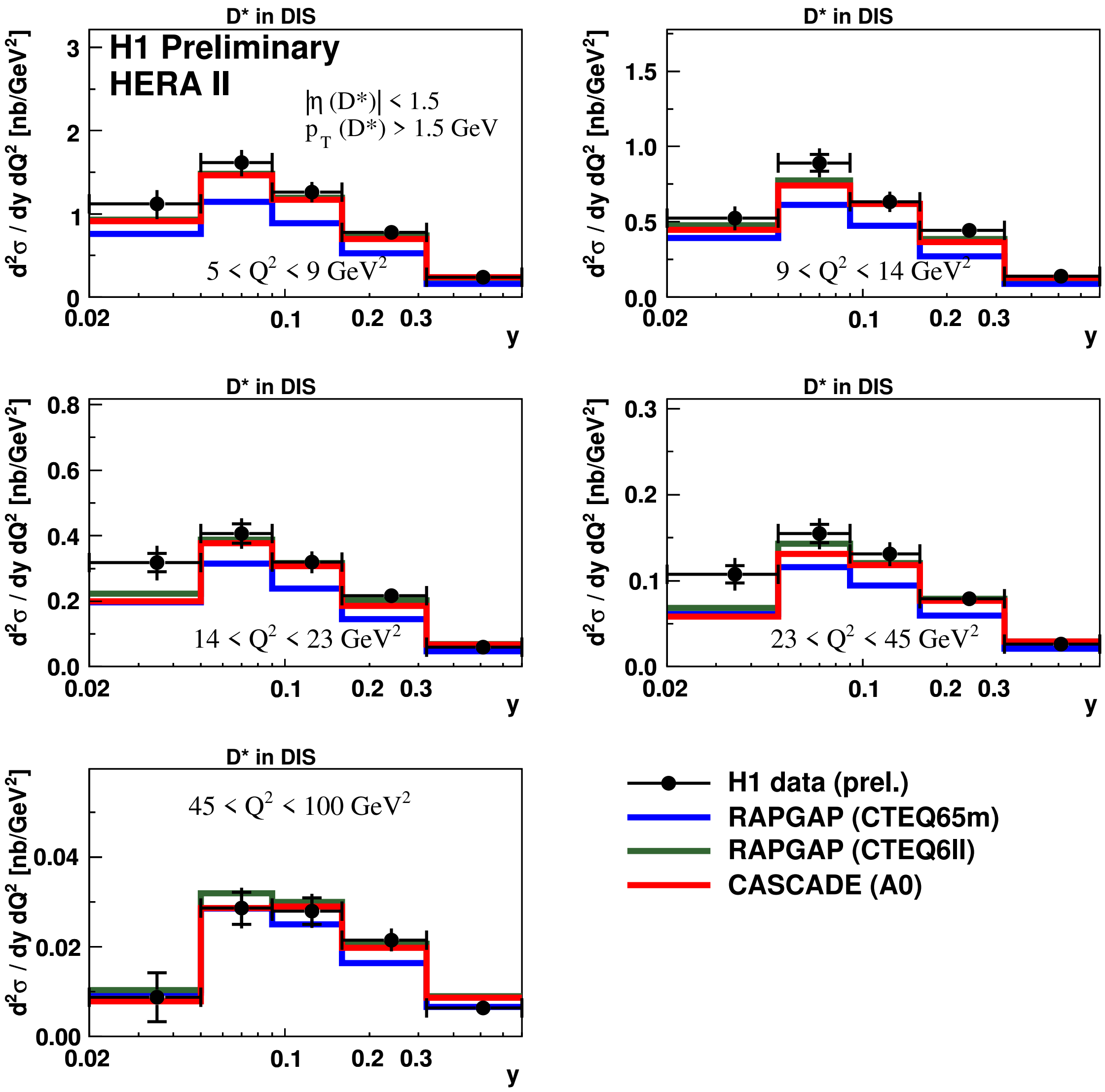

Figure 9: Double differential cross section as a function of inelasticity y and the virtuality Q_e^2 compared with RAPGAP using two different Proton PDF's and CASCADE.

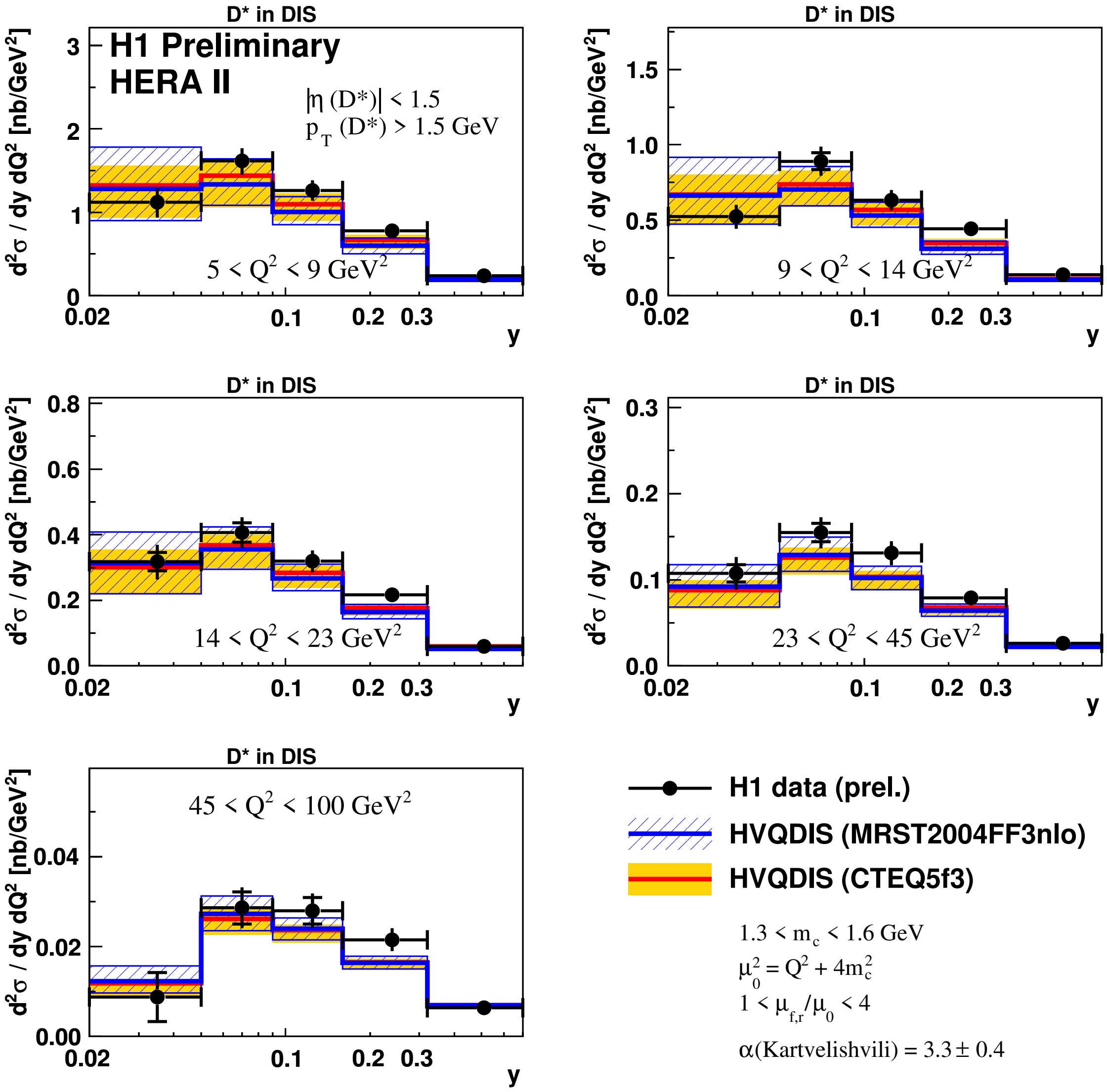

Figure 10: Double differential cross sections as a function of inelasticity y and the virtuality Q_e^2 compared with the NLO calculation (HVQDIS) with two different Proton PDF's.

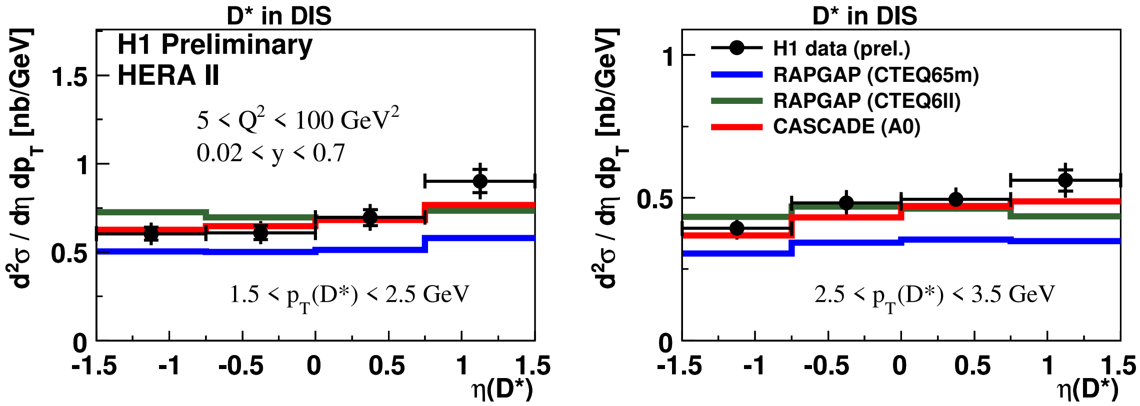

Figure 11: Double differential cross section as a function of p_T and η of the D^*-mesons compared with RAPGAP using two different Proton PDF's and CASCADE.

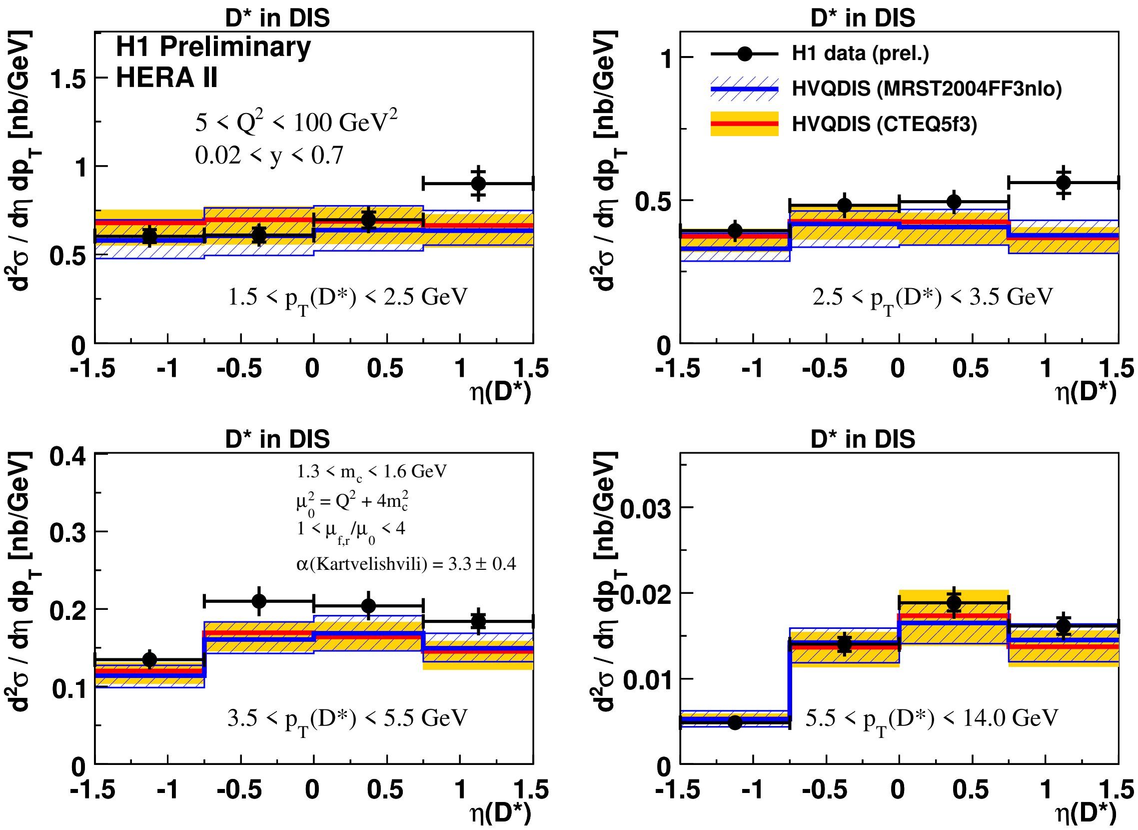

Figure 12: Double differential cross section as a function of p_T and η of the D^*-mesons compared with the NLO calculation (HVQDIS) with two different Proton PDF's.